Available online at www.sciencedirect.com
ScienceDirect
Journal of Pharmaceutical and Biomedical Analysis 42 (2006) 25–31
JOURNAL OF PHARMACEUTICAL AND BIOMEDICAL ANALYSIS
www.elsevier.com/locate/jpba

Physical and thermal characterisation of chiral omeprazole sodium salts

Nov Markovic [a], Snezana Agotonovic-Kustrin [b,*], Beverley Glass [c], Clive A. Prestidge [a]

[a] *Ian Wark Research Institute, ARC Special Research Centre, University of South Australia, Mawson Lakes Blvd., Mawson Lakes, SA 5095, Australia*
[b] *Pharmacy M315, School of Biomedical, Bimolecular and Chemical Sciences, The University of Western Australia, 35 Stirling Highway, Crawley, WA 6009, Australia*
[c] *School of Pharmacy and Molecular Science, James Cook University, Townsville, Qld 4811, Australia*

Received 22 September 2005; received in revised form 14 December 2005; accepted 16 December 2005
Available online 9 March 2006

Abstract

The physical properties of drug substances may affect stability, manufacturing, dissolution and bioavailability. Variations in the degree of crystallinity in a pharmaceutical substance may exhibit physicochemical differences that impact at therapeutic, manufacturing, commercial and legal levels, yet no reference has been found on the physical properties of micronised omeprazole. This study reports on the physical and thermal characterisation of the sodium salts of *S*- and *R*-omeprazole, using diffuse reflectance infrared Fourier transform spectroscopy (DRIFT), scanning electron microscopy (SEM), differential scanning calorimetry (DSC), microthermal analysis (μTA) and powder X-ray diffraction (XRPD). DSC experiments were performed in order to determine not only their thermal stability, but also the thermal history of both forms. SEM results indicate similar morphology, particle size and shape of powdered drug, while, μTA of processed discs shows different topographical images for *S*- and *R*-omeprazole, exhibiting a smoother surface for the *S*-form, indicative of the smoother particle size not evident in the SEM results. The low level of crystallinity of both enantiomers was confirmed by DRIFT spectroscopy and XRPD. Thermal stability by DSC of *S*- and *R*-omeprazole sodium salts was superior to that of the neutral omeprazole. This study has examined the physical and thermal properties of both forms and in highlighting their differences provides an explanation for the potential differences in bioavailability and therapeutic efficacy.

Keywords: Crystallinity; Enantiomers; Physical and thermal characterisation; Omeprazole sodium

1. Introduction

Omeprazole (5-methoxy-2-2-(4-methoxy-3,5-dimethyl-2-pyridinyl-methyl-sulfinyl)-1H-benzimidazole) is a proton pump inhibitor used to treat acid reflux disease and gastric ulcers. Formulation thus presents a challenge, due to the rapid decomposition at acidic and neutral pHs. Omeprazole is also sensitive to heat, moisture, organic solvents, and, to some degree, light. The stability of omeprazole capsules containing enteric coated pellets has been investigated with all seven products tested containing >90% of the labelled amount of omeprazole. A correlation was however found between the degree of darkening and decreased drug content in the pellets [1]. In the case of a liquid formulation of omeprazole extemporaneously prepared, the rate of degradation was temperature dependant, with the formulation remaining stable (>90%) for 30 days only at 5 °C, while the drug content declined to below 90% after only 18 days at room temperature (25 °C) [2].

Improving the bioavailability of omeprazole was originally attempted by altering the substituent pattern on the heterocyclic rings, but the real breakthrough was achieved when (*S*)-(−)-enantiomer, later named esomeprazole, was introduced onto the market by Astra Zeneca who aimed to achieve therapeutic benefit due to less inter-individual variation (slow metabolizers versus rapid metabolizers), and higher average plasma levels, providing greater dose efficiency in patients [3]. Both *S*- and *R*-omeprazole are pro-drugs, which are converted within the parietal cells to the active proton pump inhibitor, which is not a chiral molecule. While both the *S*- and *R*-forms exhibit the same effect at the active site, lower doses of *S*-omeprazole can be used to produce equivalent acid suppression as compared to racemic omeprazole. *S*-Omeprazole was introduced as the magnesium trihydrate salt first in Europe (in 2000) and later in the US (in 2001) under the trade name, Nexium®. Healing of reflux

* Corresponding author. Tel.: +61 8 6488 3199; fax: +61 8 6488 1025.
E-mail address: nkustrin@cyllene.uwa.edu.au (S. Agotonovic-Kustrin).

0731-7085/$ – see front matter © 2006 Elsevier B.V. All rights reserved.
doi:10.1016/j.jpba.2005.12.039

oesophagitis with a 40 mg day^{-1} dose of *S*-omeprazole magnesium occurred in ∼78% of patients after 4 weeks of treatment and in 93% of patients after 8 weeks, compared with 65 and 87% of patients, respectively, treated with 20 mg day^{-1} of omeprazole [4–7].

The biological and chemical properties of a drug substance can easily overshadow the importance of the bulk physical properties, yet no reference has been found on the physical properties of micronised omeprazole. Nevertheless, the effective delivery of solid pharmaceuticals is directly related to the form of the drug substance in the solid state. Variations in the degree of crystallinity in a pharmaceutical substance may exhibit physicochemical differences that impact at therapeutic, manufacturing, commercial and legal levels. Drug substances are rarely crystallised at the optimum size, and often secondary processing such as jet milling is required that may induce the formation of amorphous regions in solid drugs and excipients [8]. Generation of amorphous material during processing may also result in significant changes in the behaviour of the system [9]. The aim of this study was to assess the surface properties, particle size, shape, amorphous content and crystallinity of two omeprazole sodium enantiomers and to estimate thermal history and stability.

The characterisation of bulk drug may be performed with a range of methods. Amongst the different techniques, atomic force microscopy (AFM), as derived from scanning probe microscopy by Binning et al. [10], can be combined with thermal capabilities for surface analysis, as reviewed by Giron [11]. Many pharmaceutical systems/drugs as well as excipients have been investigated over the past 10 years using microthermal analysis (μTA): indomethacin [12,13], ibuprofen [14], pyridoxal hydrochloride [15], paracetamol [16], progesterone [17], cimetidine [18], etc. μTA is often complimentary to bulk measurement techniques such as microcalorimetry [19] or DSC [15]. In this study we have combined information from DRIFT spectroscopy, SEM, DSC, μTA and XRPD to evaluate the physical and thermal properties of the sodium salts of omeprazole stereoisomers.

2. Materials and methods

2.1. Materials

Omeprazole sodium (H199/19 sodium and H199/18 sodium); reference standards for *R*- and *S*-omeprazole (99.4%, w/w, drug purity, 99.9% isomeric purity) were kindly donated by Astra Zeneca, Sweden.

2.2. Diffuse reflectance infrared Fourier transform spectroscopy (DRIFT)

DRIFT spectra were examined over the range of 400–4000 cm^{-1} using a Nexus 670 spectrophotometer from Nicolet and spectra were recorded with the Nicolet's OMNIC software, by averaging 64 scans for each spectrum with resolutions of 4 cm^{-1} (data point resolution/interval of 1 cm^{-1}). Background spectra were obtained for each experimental condition. The intensities of the IR bands are displayed in Kubelka–Munk (K-M) units [20]. Sample mixtures were prepared by dispersing 5% (w/w) of the bulk drug in potassium bromide (KBr) (AR grade, BDH Laboratory Suppliers, Poole, UK) and mixing for 10 s in a dental amalgator (WIGL-BUG). Samples were then placed in the large sample cup (approximately 300 mg), using the supplied sample cup holder.

2.3. Scanning electron microscopy (SEM)

SEM photographs of the bulk powders were taken using a JEOL JSM-541QLV Scanning Microscope (JEOL Datum Co., Japan) with an accelerating voltage of 10 kV. Samples were mounted on a metal stub with a double-sided adhesive tape and then coated under vacuum (in an ion-sputter JFC-1100 JEOL Datum Co., Japan) with a gold layer of 200 Å in thickness.

2.4. Microthermal analysis

μTA was conducted using a μTA 2990 Micro-Thermal Analyser (TA Instruments, New Castle, DE) with a thermal probe. The thermal response of the probe was first calibrated using benzoic acid crystals (TA Instruments) with a melting point of 122 °C. Omeprazole disks of ∼1 cm in diameter were prepared by placing approximately 200 mg of powder sample into a die (routinely used in FTIR) and applying pressure of 7 tonnes for 5 min. Isothermal imaging was performed on the disks positioned on a metallic sample stage using double-sided non-conductive tape. A constant force equivalent to ∼10 nA of sensor deflection was applied and the tip rastered over an area of 100 μm × 100 μm with a scanning rate of 100 μm s^{-1} (resolution of 300 lines). Scans were performed in triplicate, at 30 °C, with a scan rate of 1 Hz and with standard error not exceeding 7%. Additionally after selecting five points on the surface area, so called localized thermal analysis (LTA), at a heating rate of 10 °C s^{-1} for up to 300 °C, was applied and reproducibility confirmed by comparing average runs and standard deviation not exceeding 5%. Burning the tip for up to 500 °C automatically cleaned the probe from any residue [21].

2.5. Differential scanning calorimetry (DSC)

DSC measurements were conducted using a DSC 2920 instrument (TA Instruments). Calibrations of base line, cell constant and temperature were performed prior to each measurement using indium (TA Instruments) with corresponding heating rates. The samples (∼4 mg) were encapsulated in a hermetically sealed aluminium pans. Samples were heated from 30 to ∼180 °C, cooled to 30 °C and then reheated in order to investigate their thermal history. For thermal stability investigations, the heating rate was 0.5 °C min^{-1} for up to 300 °C. All experiments were performed under a nitrogen purge gas rate of 50 ml min^{-1}, in duplicate with only average runs reported (standard error not exceeding 5%).

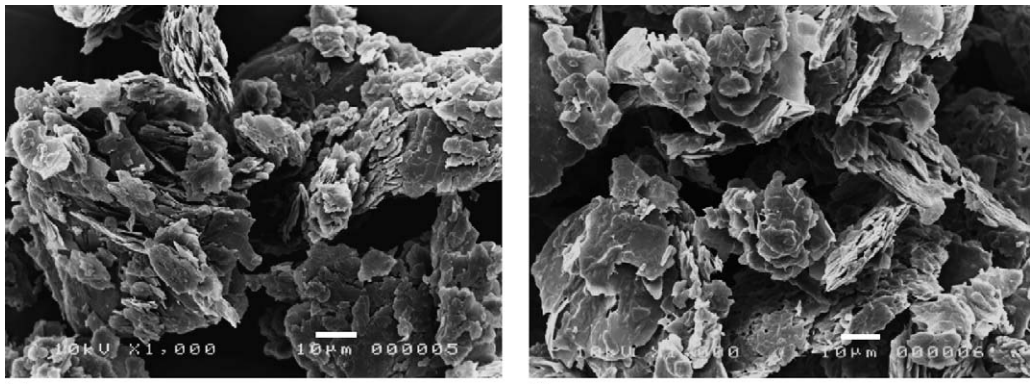

Fig. 1. SEM micrographs of powders (a) *S*-omeprazole and (b) *R*-omeprazole; bars 10 μm.

2.6. Powder X-ray diffraction (XRPD)

The samples were prepared as powder mounts: approximately 0.5 g of sample was crushed lightly in an agate mortar with a pestle and packed into a plastic cavity mount suitable for insertion. Data for the samples were collected with a Siemens D5000 front-loading X-ray diffractometer. This instrument is fitted with a copper tube (Cu Kα = 1.54178 Å), operating at 30 kV and 20 mA, and a post diffraction graphite monochromator. The sample was scanned from 1.3° to 65° 2θ in steps of 0.2° 2θ for 2.4 s per step.

3. Results and discussion

The particle size and shape of the test drugs were firstly evaluated by SEM and the results are presented in Fig. 1a and b. Both enantiomers were shown to have similar morphology, particle shape and size (in the micrometre range). Quantifying the microstructures of solid samples presents a great challenge. Since micronisation and other processing techniques can cause changes in the crystallinity of powders, we decided to investigate the level of crystallinity of micronised omeprazole.

The level of crystallinity of the omeprazole enantiomers was examined and a low level confirmed by DRIFT analysis (Fig. 2). The intensity of bands was as expected low, at less than seven Kubelka–Munk units (due to a low refractive index). Although many materials contain both crystalline and non-crystalline phases, a key characteristic of such semi-crystalline materials is the degree of crystallinity (Ic). The IR spectrum is sensitive to the level of order/disorder in the crystal structure of the sample. The index Ic can be calculated as a ratio of intensities of absorption bands at 1372 cm^{-1} for the deformational oscillations of CH groups (disorder) and covalent vibrations of CH_2 and CH groups at ~2900 cm^{-1} (order) [22]. Ordered CH vibrations seemed to increase slightly whereas deformational CH absorbance increased sharply with the increase of *S*-omeprazole proportion in physical mixture. The crystallinity indices were calculated to be 1.81 and 1.18 for *S*- and *R*-omeprazole, respectively (these values are relatively low as expected). For comparison purpose the change in Ic ratio is presented as a function of the *S*-omeprazole content in physical mixture (Fig. 3).

The degree of crystallinity affects molecular vibration due to the change in molecular symmetry. Since the symmetry of a molecule is higher in the amorphous form, certain types of vibrations are inactive in this form. In addition, variation in particle size can have a significant influence on the DRIFT measurements [23]. Defects in the microstructure, which are due to the preparation technique, may lead to spectral changes. Although grinding can reduce the variation in particle size, in our case this was avoided because of the requirement to analyse directly the powdered samples with minimal pretreatment. Results showed the band intensity of *R*-omeprazole to be decreased due to increased particle size [24].

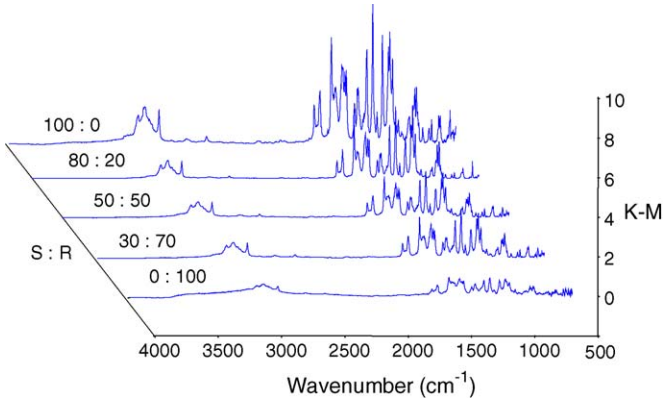

Fig. 2. DRIFT spectra as a function of the *S*-omeprazole:*R*-omeprazole (w/w) ratio in physical mixtures.

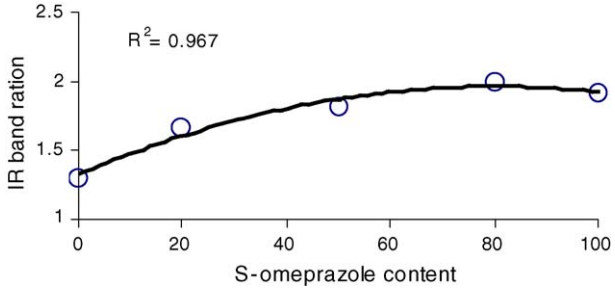

Fig. 3. Ratio of the IR bands (Ic) as a function of the *S*-omeprazole content in physical mixtures.

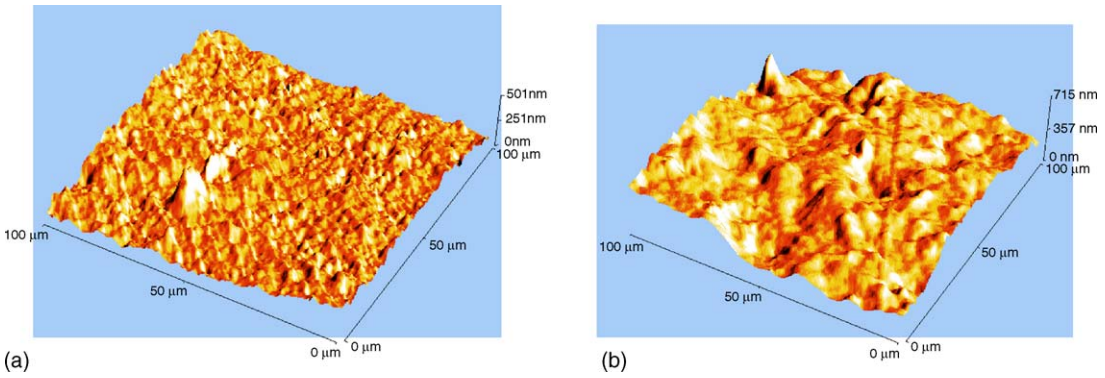

Fig. 4. Surface topographical images of compressed disks of: (a) *S*-omeprazole and (b) *R*-omeprazole.

Samples were further studied using μTA (drug disks) and by DSC (powder form) in order to further differentiate between amorphous and crystalline forms. μTA simultaneously acquires and display images of the sample's topography, thermal conductivity and thermal diffusivity. Subsequently, it can perform a differential surface thermal analysis and thermomechanical analysis on a micron scale within the sample. Initially the sample disks were imaged using μTA (Fig. 4) so that the relevant areas could be further selected for local thermal analysis.

Fig. 4 shows the topographical images, illustrating the difference of the disposition of *S*- and *R*-omeprazole on a surface. No evidence of sample deformation or tip degradation was observed during imaging. The *S*-omeprazole image (100 μm × 100 μm) clearly shows the surface to be of closely packed uniform particles and smoother than that of the surface of *R*-omeprazole. The roughness was caused by the compaction of the powder particles and by the deformation of particles under compression. Surface roughness was calculated by μTA Lab software (TA Instruments) in terms of the percentage difference for the particle height distribution (Table 1). In the case of *S*-omeprazole 65% of the surface height was up to 200 nm and 35% was from 200 to 300 nm. In the case of *R*-omeprazole 19% was up to 200 nm, 63% from 200 to 400 nm and remaining 18% was higher than 400 nm, which if compared to *S*-omeprazole gave a rough height distribution. The fact that μTA measures roughness in a small area (10^4 μm^2), should be taken into account.

Global measurements of the texture that is observed in an image can provide information about the size of the particles [25]. Smaller particles lead to finer textures and larger particles to coarser textures, as described by Russ [26]. In order to further explore the possibility of differentiating between the amorphous and crystalline phases using thermal conductivity, 2D topography and thermal conductivity images with corresponding pixel intensity histograms of *S*- and *R*-omeprazole were considered and are presented in Figs. 5 and 6. The surface topography may have a profound effect on the thermal conductivity signal resulting in peaks appearing as low conductivity (dark) areas and troughs as high conductivity (light) areas. Topographical images reveal only the quality of the surface after sample preparation. *S*- and *R*-omeprazole have visibly different topographical images with a mean roughness of 122 and 201 nm, respectively. However, both isomers show similar multimodal height distribution, reflecting the fact that there is a systematic topographic differentiation in height within isomers due to the presence of amorphous and microcrystalline phases. As expected the *S*-omeprazole histogram shows less roughness and thus better quality of the surface after sample preparation. The thermal conductivity histograms show a clear monomodal distribution, adding strength to the argument that we have only one compound present and that conductivity is not a simple reflection of topography.

Localized thermal analysis measures surface thermal responses within an area of only a few square microns in direct contact with the surface. Changes in thermal conductivity across the surface results in a different heat flow between the probe tip and sample. In addition to deflection data, the power level necessary to keep the heating rate constant (relatively to reference probe) may be monitored for the endothermic transitions associated with melting and/or exothermic events related to glass transitions or crystallizations processes. The derivative of the power signal (dW/dt) is used to aid data analysis and to identify exothermic and endothermic events (Fig. 7). These LTA were

Table 1
Height distribution (as estimated by mTA) for compressed disks of *R*- and *S*-omeprazole

Omeprazole			Esomeprazole		
Height (nm)	Average height	Percent	Height (nm)	Average height	Percent
<200	54.7	18.3	<50	3.0	1.0
200–250	110.0	36.8	50–100	32.7	10.9
250–300	76.7	25.6	100–150	71.7	24.0
300–350	31.7	10.6	150–200	82.0	27.4
350–400	9.3	3.1	200–250	92.3	30.9
>400	13.0	4.4	>250	14.0	4.7

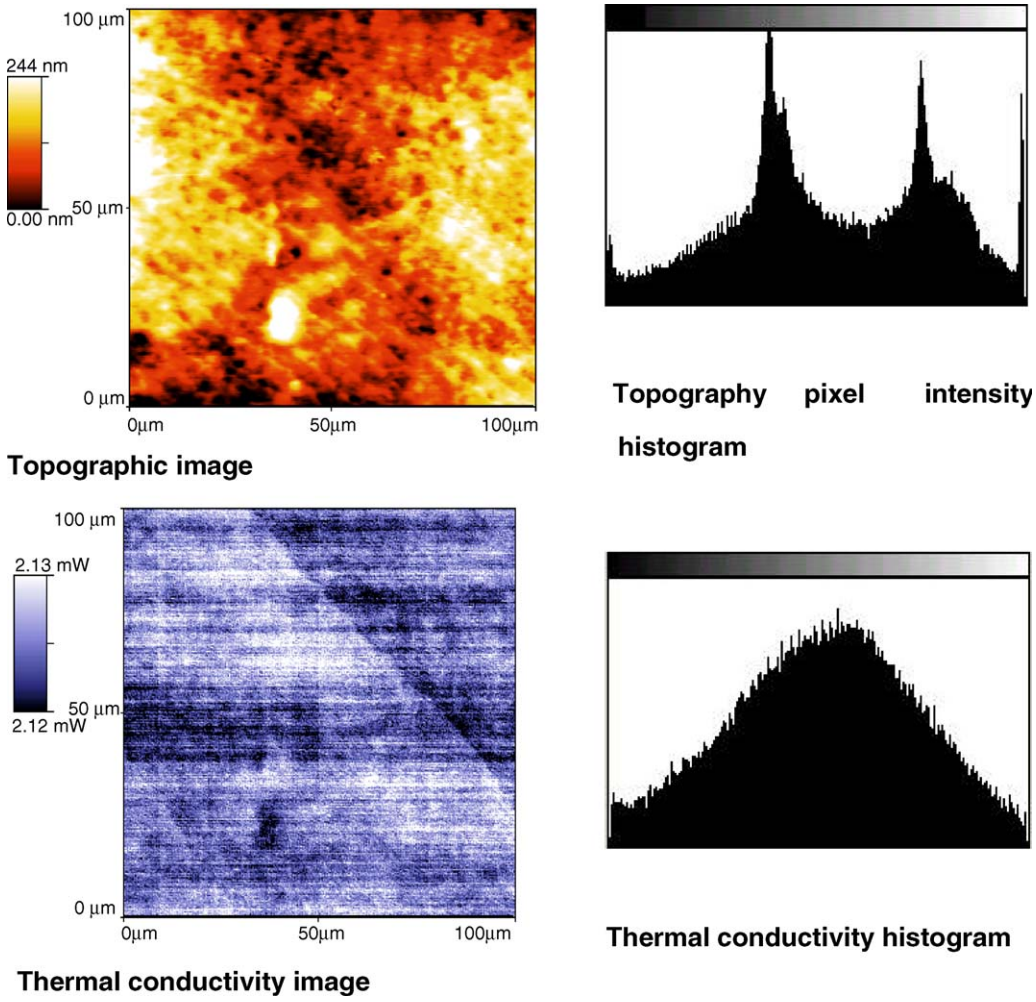

Fig. 5. *S*-Omeprazole: topography pixel image and thermal conductivity image with corresponding intensity histograms.

examined and later compared with the bulk properties using DSC.

During LTA of both samples, a constant increase in power consumption is observed up to 151 °C (*R*-omeprazole) and 126 °C (*S*-omeprazole). A sharp decrease in power was recorded with the further heating. This is related to an exothermic event and probably to the total dehydration of the samples. Immediately after dehydration a sharp increase in power consumption (endothermic event) was evident and is related to melting at ∼160 °C for the *R*-form and at ∼156 °C for the *S*-form, respectively. Further heating induced a sharp exothermic peak (at 167 °C) for *R*-omeprazole, higher in comparison to the peak at around 165 °C for *S*-omeprazole, indicating a recrystallization process.

In order to clarify the thermal stability of both omeprazole forms, a detailed thermal history of both samples was examined by applying a heating ramp of 0.5 °C min^{-1} (from 30 to 300 °C) (Fig. 8). It was noticeable that DSC did not observe thermal peaks in the thermal range between 150 and 170 °C. The melting temperature could not be detected due to the predominant amorphous nature of the samples. However, degradation peaks at 229.5 and 227 °C for *R*- and *S*-omeprazole sodium salts were reproducible for both forms within experimental limits. These peaks are assigned to degradation of omeprazole and are an indication that these sodium salts are more stable forms if this data are compared to reported literature values [27,28] for the neutral form of omeprazole. Samples were cooled down, isothermally held at 30 °C for 30 min, than reheated to 300 °C (not shown). No thermal changes could be detected meaning that thermal history of the samples was completely removed.

The XRPDs for *R*- and *S*-omeprazole are presented in Fig. 9, with both enantiomers showing a low level of crystallinity as confirmed by DRIFT spectroscopy. These results also concur with the level of crystallinity and crystallinity indices as determined by DRIFT spectroscopy. The presence of an amorphous fraction within microcrystalline samples may result in noticeably different behaviour from that of a completely amorphous material, particularly in terms of recrystallization, with recrystallization being highly dependent on the molecular mobility of the amorphous phase. Current interest in pharmaceutical industry to quantify the proportion of amorphous material is potentially misleading, as the nature of such material may contribute equally or to an even greater extent to product performance [29]. Our attempts are to quantify the proportion of amorphous material within a microcrystalline phase, assuming that the amorphous fraction is essentially comparable to wholly amorphous material.

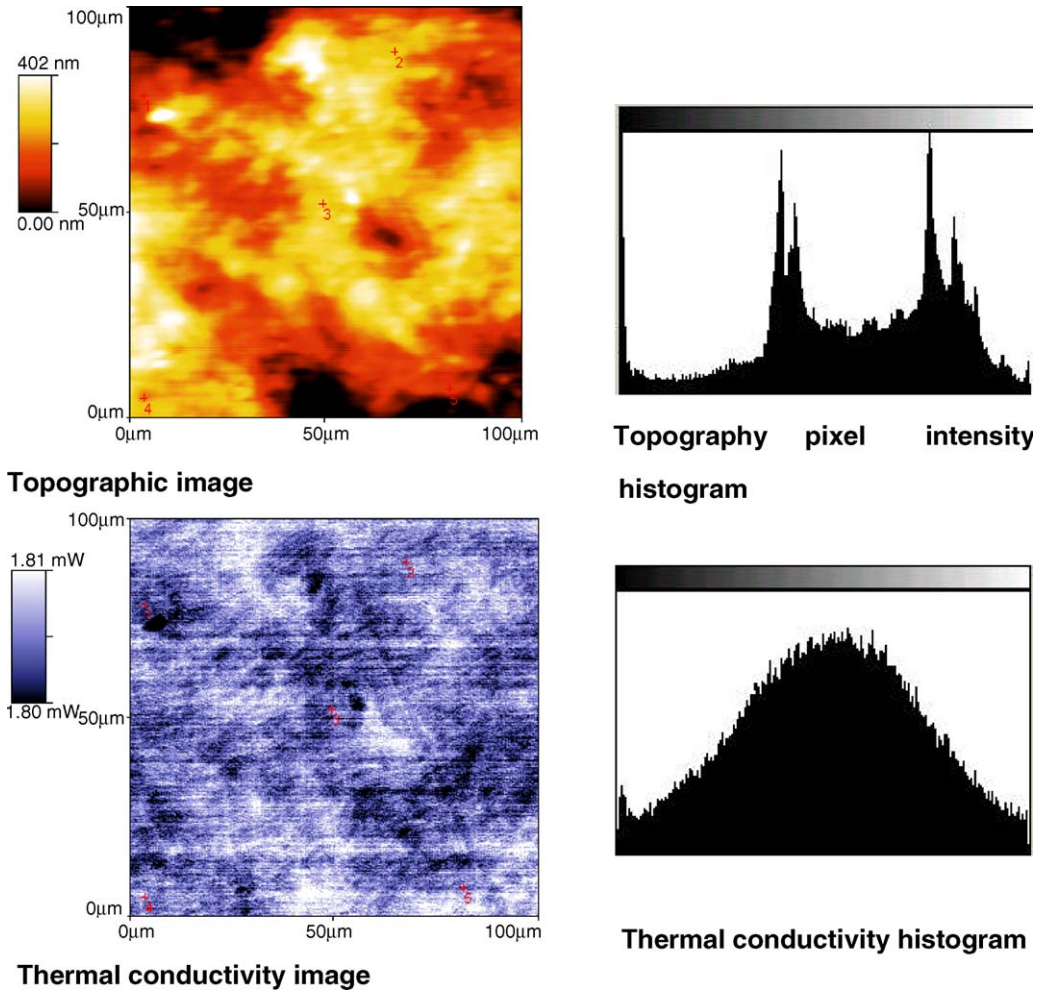

Fig. 6. *R*-Omeprazole: topography pixel image and thermal conductivity image with corresponding intensity histograms.

Clearly, in theory, an infinite number of amorphous states may be generated under different experimental conditions. However, for most pharmaceutical systems, there is a general acceptance of the two-phase model of a semi-crystalline material containing a proportion of amorphous material. In such systems, molecular mobility is restrained to a greater extent than in the perfect amorphous state, thus exhibiting intermediate properties [11,30].

As the material is heated through the melting point temperature, the amorphous component does not undergo the mobility change of the microcrystalline component. Consequently, the amorphous fraction does not contribute to the heat capacity change at the glass transition leading to discrepancies between

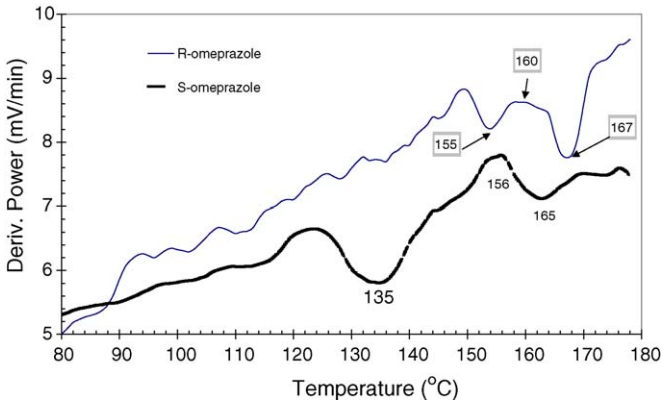

Fig. 7. µTA (LTA) overlaid runs of *S*- and *R*-omeprazole for changes of derivative of power.

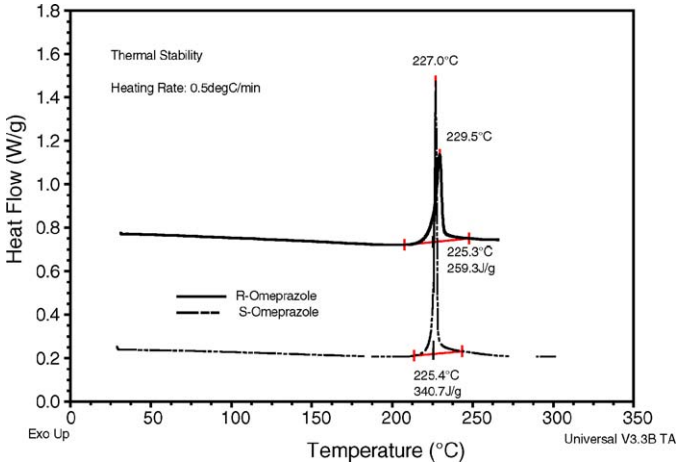

Fig. 8. DSC curves of *R*- and *S*-omeprazole forms (heating ramp of 0.5 °C min^{-1}).

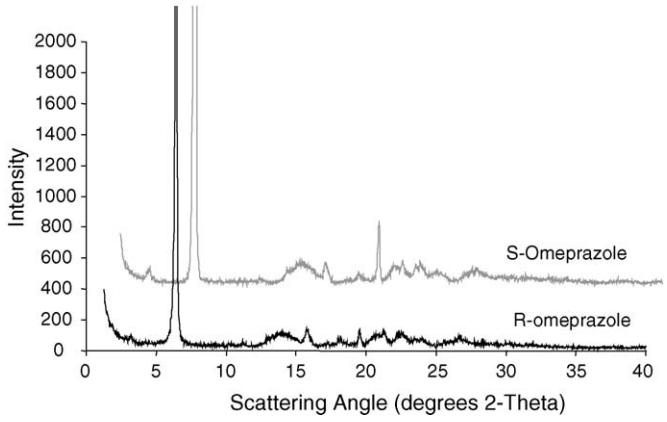

Fig. 9. Comparative XRPD of *R*- and *S*-omeprazole.

the degree of crystallinity calculated from the DSC results and that from the data obtained using IR spectroscopy [31].

4. Conclusions

Literature report on the instability of omeprazole in an acidic medium, to heat, moisture and light, necessitating the inclusion of sodium bicarbonate in extemporaneously prepared liquid formulations and storage at 5 °C limited to 30 days. *S*-Omeprazole when introduced onto the market produced efficacy at lower doses and healing of oesophagitis in a greater percentage of patients as compared to the racemate. It is important to understand whether this is due to administration of the drug substance as the pure enantiomer, the physical properties of this enantiomer or both. Micronisation of a drug substance can improve dosage form characteristics by enhancing dissolution rates and hygroscopicity and consequently increase bioavailability. Smaller and more uniform particle size of esomeprazole were evidenced in SEM photo, confirmed by XRPD and by the increase in the IR band intensity and smoother surface of closely packed uniform particles in the topographical image for *S*-omeprazole. Despite these differences the presence of an amorphous and microcrystalline phase was detected in both forms. Particle size reduction processes commonly introduce amorphous domains that have a disproportional effect on physical stability. In the case of omeprazole introducing its sodium salts could solve this problem. Higher degradation peaks measured with DSC, at 229.5 and 227 °C for *R*- and *S*-omeprazole sodium salts, indicated that the sodium salts are more stable forms if compared to reported literature values for the corresponding neutral form of omeprazole. Presentation of the results of these physical and thermal characterisations of these forms highlighting their differences provides the pharmaceutical scientists with insight into their bioavailability and therapeutic efficacy.

Acknowledgements

The authors wish to acknowledge the financial support of the Ian Wark Institute from the University of South Australia and James Cook University, Qld, Australia. The authors also wish to recognise the contribution of Dr. Britt-Marie Jacobson of Astra Zeneca, Sweden for her input and for providing pure drug compounds.

References

[1] M. Palummo, A. Cingolani, L. Dall, M.G. Volonte, Boll. Chim. Farm. 139 (2000) 124–128.
[2] R.A. Quercia, C. Fan, X. Liu, M.S. Chow, Am. J. Health Syst. Pharm. 54 (1997) 1833–1836.
[3] E. Chong, M.H. Ensom, Pharmacotherapy 23 (2003) 460–471.
[4] L. Olbe, E. Carlsson, P. Lindberg, Nat. Rev. Drug Discov. 2 (2003) 132–139.
[5] P.B. Kale-Pradhan, H.K. Landry, W.T. Sypula, Ann. Pharmacother. 36 (2002) 655–663.
[6] K. Rohss, G. Hasselgren, H. Hedenstrom, Digest. Dis. Sci. 47 (2002) 954–958.
[7] P. Lindberg, D. Keeling, J. Fryklund, T. Andersson, P. Lundborg, E. Carlsson, Aliment. Pharmacol. Ther. 17 (2003) 481–488.
[8] S. Gaisford, G. Buckton, Thermochim. Acta 380 (2001) 185–198.
[9] C. Ahlneck, G. Zografi, Int. J. Pharm. 62 (1990) 87–95.
[10] G. Binning, C.F. Quate, C.H. Gerber, Phys. Rev. Lett. 56 (1986) 930–933.
[11] D. Giron, J. Therm. Anal. Calorim. 68 (2002) 335–357.
[12] H.M. Pollock, A. Hammiche, J. Phys. D: Appl. Phys. 34 (2001) R23–R53.
[13] P.G. Royall, V.L. Kett, C.S. Andrews, D.Q.M. Craig, J. Phys. Chem. B 105 (2001) 7021–7026.
[14] J.R. Murphy, C.S. Andrews, D.Q.M. Craig, Pharm. Res. 20 (2003) 500–507.
[15] L. Bond, S. Allen, M.C. Davies, C.J. Roberts, A.P. Shivji, S.J.B. Tendler, P.M. Williams, J. Zhang, Int. J. Pharm. 243 (2002) 71–82.
[16] D.M. Price, M. Reading, A. Hammiche, H.M. Pollock, Int. J. Pharm. 192 (1999) 85–96.
[17] P.G. Royall, V.L. Hill, D.Q.M. Craig, D.M. Price, M. Reading, Pharm. Res. 18 (2001) 294–298.
[18] G.H.W. Sanders, C.J. Roberts, A. Danesh, A.J. Murray, D.M. Price, M.C. Davies, S.J.B. Tendler, M.J. Wilkins, J. Microsc. 198 (2000) 77–81.
[19] H. Ahmed, G. Buckton, D.A. Rawlins, Int. J. Pharm. 130 (1996) 195–201.
[20] P.R. Griffiths, M.P. Fuller, in: R.E. Hester, R.J.H. Clark (Eds.), Advances in Infrared and Raman Spectroscopy, Heyden, London, 1981.
[21] TA Instruments μTA 2990 Micro Thermal Analyser Operator's Manual, TA Instruments Inc., New Castle, DE, 1999.
[22] M.L. Nelson, R.T. O'Connor, J. Appl. Polym. Sci. 8 (1964) 1311–1341.
[23] M.P. Fuller, P.R. Griffiths, Anal. Chem. 50 (1978) 1906–1910.
[24] H. Wang, C.K. Mann, T.J. Wickers, Appl. Spectrosc. 56 (2002) 1538–1544.
[25] B. Novales, S. Guillaume, M.F. Devaux, M. Chaurand, J. Sci. Food Agric. 78 (1998) 187–195.
[26] J. Russ, The Image Processing Handbook, third ed., CRC Press, Boca Raton, FL, 1999.
[27] S. Budavari (Ed.), The Merck Index, 12th ed., Merck Res. Lab., New Jersey, 1996.
[28] EP 1 018 340 A9: inclusion amino acid salts compounds of benzimidazole derivatives with cyclodextrins their preparation and pharmaceutical formulations containing them.
[29] D.Q.M. Craig, V.L. Kett, J.R. Murphy, D.M. Price, Pharm. Res. 18 (2001) 1081–1082.
[30] H. Suzuki, J. Grebowicz, B. Wunderlich, Br. Polym. J. 17 (1985) 1–3.
[31] V.B.F. Mathot, in: V.B.F. Mathot (Ed.), Calorimetry and Thermal Analysis of Polymers, Hanser Publishers, Munich, 1994, pp. 146–160.